ICFA INSTRUMENTATION BULLETIN*

The publication of the ICFA Instrumentation Bulletin is an activity of the Panel on Future Innovation and Development of ICFA (International Committee for Future Accelerators).

Volume 18

• Spring 1999 Issue

ICFA INSTRUMENTATION BULLETIN

The publication of the ICFA Instrumentation Bulletin is an activity of the Panel on Future Innovation and Development of ICFA (International Committee for Future Accelerators). The Bulletin reports on research and progress in the field of instrumentation with emphasis on application in the field of high-energy physics. It encourages issues of generic instrumentation.

The views expressed in this Bulletin do not necessarily represent those of the ICFA Panel or the editor. In all cases, the authors are responsible for their manuscripts. The printed version is mailed out in limited numbers to institutions on the SLAC Instrumentation mailing list. Issues of the ICFA Instrumentation Bulletin are accessible electronically on our Web site:

http://www.slac.stanford.edu/pubs/icfa/

Cover: The illustration depicts L. J. Waghenaer's marine atlas, "The Mariner's Mirror," published in 1588. Lucas Janszoon Waghenaer was born in Holland in the 1530s. He became a famous ship pilot in his time. In 1584, he published the atlas ("Spieghel der Zeevaerdt") which was greatly valued among mariners for centuries. This was not due only to the map content, but also to the detailed knowledge of navigation techniques of that time. The atlas, as it appears on our page, is the same one used for the Dutch to English translation.

Table of Contents

1999 Conference List

- VIII ICFA School on Instrumentation in Elementary Particle Physics
  June 28-July 10, 1999, University of Istanbul, Istanbul, Turkey,
  http://icfa99.istanbul.edu.tr.

- ITP Conference on Magnetic Phenomena in Novel Materials and Geometries,
  16-20 August 1999, Santa Barbara, CA, U.S.A.

- The 5th International Conference on Position Sensitive Detectors,
  September 1999, London, England.

- The 46th National Symposium of the American Vacuum Society,
  8-22 October 1999, Seattle, WA, U.S.A.

- The 11th International Workshop on Room Temperature Semiconductor X Ray and
  Gamma Ray Detectors and Associated Electronics,
  11-15 October 1999, Vienna, Austria.

- The 11th U.S. National Synchrotron Radiation Instrumentation Conference (SRI99),
  13-15 October 1999, Stanford, CA, U.S.A.

- The IEEE Nuclear Science Symposium and Medical Imaging Conference,
  26-30 October 1999, Seattle, U.S.A.

- The 7th International Conference on Instrumentation for Colliding Beam Physics (INSTR99),
  5-19 November 1999, Hamamatsu, Japan.

Production of a New Generation of Silica Aerogel

and its Application for the KEK B-Factory Experiment

T. Sumiyoshi[1]

High Energy Accelerator Research Organization (KEK)

1-1 Oho, Tsukuba, Ibaraki, 305, Japan

Abstract

Low-refractive index silica aerogel is the most convenient radiator for threshold-type Cherenkov counters, which is used for particle identification in high-energy physics experiments. For the BELLE detector at the KEK B-Factory, we have produced about 2 m^3 hydrophobic silica aerogels of n = 1.01 - 1.03 using a new production method. The particle identification capability of the aerogel Cherenkov counters was tested, and 3 σ pion/proton separation has been achieved at 3.5 GeV/c. Radiation hardness of the aerogels was confirmed up to 9.8 Mrad.

Thanks to the improved transparency, aerogels prepared by the two-step method can be used as radiators, not only as a threshold-type, but also for ring imaging-type Cherenkov counters. The newly developed aerogels will be used extensively for particle identification devices in future high-energy physics experiments.

1. Introduction

In high-energy physics experiments, the identification of particles is very important in the understanding of detailed dynamics of underlying interactions. One method for such particle identification involves detection of the Cherenkov light emitted by charged particles passing through transparent materials. This light is produced only when the velocity of the particle is faster than the velocity of light in the material. This condition is expressed as:

$$n \beta > 1, \qquad (1)$$

where n is the refractive index of the material, and β is the velocity of the charged particle in units of c (velocity of light in vacuum). Figure 1 shows $n \beta$ = 1 lines for pions and kaons. In this figure, condition (1) is satisfied for the regions above each line; hence, the hatched area is the region where pions emit Cherenkov light and kaons do not. Thus, if we select a material with n = 1.01, then only pions will emit Cherenkov light in a momentum range between 0.98 GeV/c and 3.48 GeV/c. The figure indicates that a material having a refractive index of less than 1.03 is indispensable for pion/kaon separation at a few GeV/c with a threshold-type Cherenkov detector. However, it is very difficult to attain such a low refractive index with most materials. The only candidates other than silica aerogels are liquid Helium (n = 1.024) or pressurized CO_2 (n = 1.02 at 25MP), neither of which allows for easy handling. For this reason, a large number of experiments [1] have used silica aerogels as the radiator for threshold-type Cherenkov counters. The first successful demonstration of this technique was by *Cartin et al.* in 1974 [2]. Before this

experiment, a fine grained silica powder, mixed with air, was tried to achieve a low-refractive index material [3]; however, the number of observed Cherenkov photons was quite small compared to latter silica aerogel experiments.
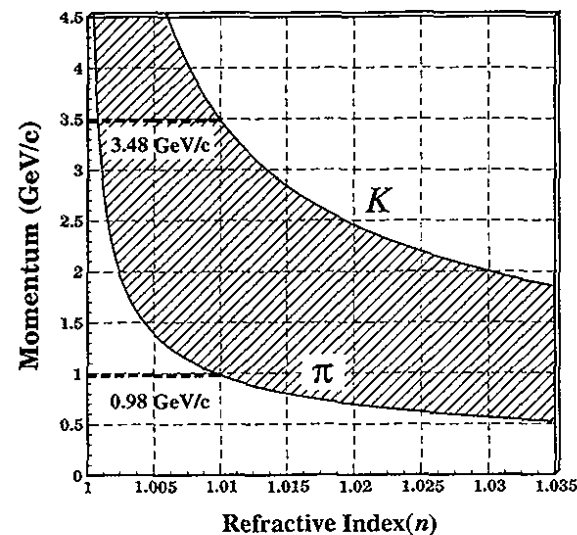

Fig. 1. In the region above each curved line ($n \beta$ = 1), particles (pions or kaons) emit Cherenkov light. The hatched area is the region where pions emit Cherenkov light and kaons do not.

Before the invention of the two-step method [4], it was very difficult to produce silica aerogels having a refractive index below 1.02. This restricted the particle identification capability to low momentum regions (p < 2.5 GeV/c). Recent *B*-physics experiments, however, require good particle identification on the momentum range of up to 4 GeV/c, and low-refractive index material (n = 1.007 to 1.03) becomes vital for such experiments. Thanks to the invention of the two-step method, silica aerogel with low-refractive index can be easily produced. We have produced about 2.0 m^3 of silica aerogel (n = 1.01 to 1.03) for the KEK B-Factory experiment [5] in a cooperative work with Matsushita Electric Works, Ltd. and KEK.

Here, we report details of our silica aerogel counter, which will be used for the KEK B-Factory experiment. Section 2 provides an outline of the silica aerogel application in the BELLE detector; Section 3 describes the production methods and the quality of the aerogel produced; Section 4 evaluates its performance. Other applications for high-energy experiments are also briefly discussed.

---

[1] Author's e-mail: takayuki.sumiyoshi@ kek.jp, tel: +81-298-64-5333, telefax: +81-298-64-2580.
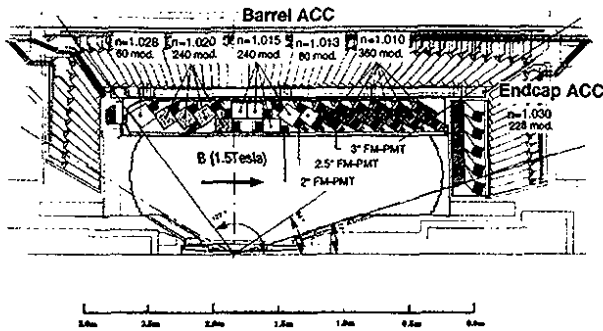
Fig. 2. The arrangement of the ACC at the center of the BELLE detector.

2. Silica Aerogel for the BELLE Detector

One of the most intriguing puzzles of nature is that the universe is composed of only matter, which contradicts cosmological theories, suggesting that an equal amount of particles and antiparticles have been produced in the Big Bang. A simple explanation of this phenomenon requires the violation of matter-antimatter symmetry (so-called CP symmetry), which has so far been only observed in the kaon system [6]. The K-M scheme [7] of the Standard Model, which is the most successful theory in particle physics, predicts a large CP asymmetry in the B-meson system [8]. In order to elucidate this interesting physics, several B-Factories have been proposed and are being constructed around the world at such places as CESR (Cornell) [9], SLAC-B (Stanford) [10], KEK-B (KEK), HERA-B (DESY) [11], and LHC-B (CERN) [12], where large numbers ($\sim 10^{7\text{-}8}$/year) of B-meson decays will be examined for the study of CP violation among other things. In such B-Factories, separation of pions from kaons is vital for the identification of B or $\bar{B}$ mesons and the selection of rare decays. The BELLE group (the experimental group for KEK B-Factory) has decided to use an array of silica aerogel Cherenkov counters (ACC) for such particle identification. Figure 2 shows the configuration of the ACC in a central part of the BELLE detector. The ACC consists of 960 counter modules for the barrel part and 228 modules for the end-cap part of the detector. In order to obtain good pion/kaon separation for the whole kinematics range, the refractive indices of aerogels are selected to be between 1.01 and 1.03, depending on their polar angle region. A view of a typical single ACC module is shown in Fig. 3. Five aerogel tiles are stacked in a thin (0.2mm thickness) aluminum box ($12\times12\times12$ cm^3). In order to effectively detect the Cherenkov light, two fine mesh-type photomultiplier tubes (PMT's) [13], which operate in a magnetic field of 1.5 T, are attached directly to the aerogels at both sides of the box. We use PMT's of three different diameters: 3" (R6683), 2.5" (R6682), and 2" (R6681) for silica aerogel of $n = 1.01$, 1.015 and 1.02, respectively. The inner surface of the box (except for the phototube windows) is lined with a diffuse reflector (Gortex sheet [14]) to obtain a uniform response. The total volume of aerogel needed for the ACC is about 2 m^3. For the study of CP

violation, the ACC is required to distinguish pions and kaons with a resolution better than 3σ.
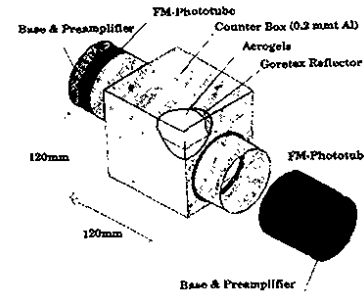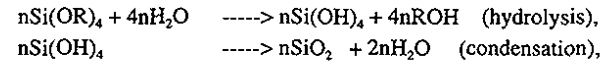

Fig. 3. Schematic drawing of a typical single ACC module: five aerogel tiles are contained in a thin aluminum box lined with a white reflector (Gortex sheet). They are viewed by two fine mesh PMT's.

3. Production of Silica Aerogels

3.1. Preparation of Alcogels

Silica aerogels are conventionally produced by the so-called "sol-gel" process, in which the gels, "alcogels," leading to high-porosity aerogels, are made from the following two reactions (hydrolysis and condensation):

$$nSi(OR)_4 + 4nH_2O \quad \text{-----} > nSi(OH)_4 + 4nROH \quad \text{(hydrolysis),}$$
$$nSi(OH)_4 \qquad \text{-----} > nSiO_2 + 2nH_2O \quad \text{(condensation),}$$

where OR represents an alkoxyl group such as CH_3O.

These two reactions take place simultaneously in an alcohol solvent with an acid or base catalyst. Then geletion proceeds and syneresis continues to strengthen the structure. The refractive index of aerogel (n), which is proportional to its density (ρ: g/cc) as $n - 1 = 0.21 \rho$, is determined by the ratio of SiO_2 and the alcohol. The amount of mixed alcohol can control the refractive index. Hence, if one wants to make a low refractive index aerogel, one needs to add larger amounts of alcohol; however, that induces the reverse reaction of hydrolysis and gelation is prevented. This is why the production of a low-refractive index aerogel with good transparency was difficult.

In order to surmount this problem, a two-step method was proposed by R. Hrubesh et al. During the first step, less water than required to complete the hydrolysis is used to obtain partially hydrolyzed silica precursor. For instance, the complete hydrolysis of one mol of tetra-alkoxysilane requires 4 mol of water; however, they only added 1.3 mol of water. Later on, all the alcohol is distilled off, and the remaining silica precursor is diluted by a solvent without alcohol, such as acetonitril. In the second step, the silica oil thus produced is further processed to make a gel by adding extra water with a base catalyst. By adopting such a procedure, the reverse reaction of hydrolysis is inhibited, and we can make a silica aerogel with porosity as high as 99.9% or more. The silica aerogel thus produced has a different microstructure from that of conventionally produced ones, namely having a much smaller pore size.
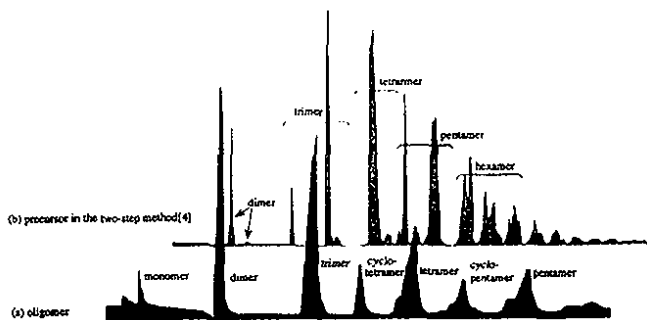
Fig. 4. Charts for the (a) oligomer and (b) precursor measured by a gas chromatograph mass spectrometer. The horizontal and vertical directions correspond to the response of time and the content of each composition, respectively.

Table 1. The molar mixing ratios for the preparation of alcogels of four different indices (n = 1.01, 1.015, 1.02, and 1.028). Here, we assume that the molecular weight of MS51 is 470. We used methanol as the solution for n = 1.028 alcogels.

Refractive index	MS51	ethanol	water	NH$_3$
1.01	1	139.7	18.25	2.466
1.015	1	89.66	21.57	0.8324
1.02	1	57.56	25.48	0.2810
1.028	1	56.95	25.06	0.1578
		(methanol)		

We adopted a modified two-step method for the preparation of alcogels, in which we used a methylalkoxide oligomer as the precursor instead of using the partially hydrolyzed silica precursor. This oligomer contains 51% silica (SiO$_2$) in percentage weight and is commercially available ("Methylsilicates-51" by Colcoat Co., Ltd.). Using a gas chromatograph and mass spectrometer, the composition of this oligomer was compared with the precursor that is used in the standard two-step method, and was found to be very similar to the latter, as shown in Fig. 4. This oligomer is hydrolyzed and polymerized in a basic catalyst (NH$_4$OH) with a solution of methanol or ethanol. Although this method is not exactly the same, we can take advantage of the standard two-step methods and produce a low-refractive index aerogel. This method is suitable for mass production of aerogel, since we can eliminate the complicated process in the first step of the standard two-step method: alcohol distilled and diluted with acetonitril, etc.

The average size of the produced alcogels are 120 x 120 x 24 mm^3. They are formed in aluminum molds coated with a thin PTFE film. The molar mixing ratios of the oligomer,

methanol (ethanol), water, and ammonia are optimized so that the transmittance of dried aerogels are as high as possible. The molar mixing ratios of the materials are summarized in Table 1. The typical gelation time ranges from a few to 10 minutes, depending on the densities. For aerogels with densities greater than 0.1g/cc, we adopted a methanol solution instead of ethanol, for better transparency.

3.2. Surface Modification for a Hydrophobic Property

Silica aerogels have been used in several experiments; however, their transparencies became worse within a few years of use [15]. This phenomenon may be attributed to the hydrophilic property of the silica aerogels. In order to prevent such effects, we have made our silica aerogels highly hydrophobic by changing the surface hydroxyl groups into trimethylsilyl groups [16]. This modification can be done at any one of the three stages: before the drying, while drying, or after the drying; we adopted the first option for simplicity. After one week of aging, the alcogels are submerged into a solution for three days, consisting of a mixture of hexamethyldisilazane and ethanol with a volume ratio of 1:8. As a result of this treatment, our silica aerogels are still as transparent as when they were produced about two and a half years ago. Since such processed aerogels are highly hydrophobic, these aerogels are easily shaped into any form by using a water-jet cutter without any damage to the transparency.

3.3. Drying

After three weeks of aging, including the surface modification, the alcogels are dried with CO$_2$. Figure 5 shows a flow sheet of our drying facility. The autoclave volume is 140 litres (550 mm in diameter and 590 mm in height), and can produce about 38 litres of silica aerogel in one batch. After seven months of operation (two batches/week), we have completed the production of about 2 m^3 of silica aerogels.
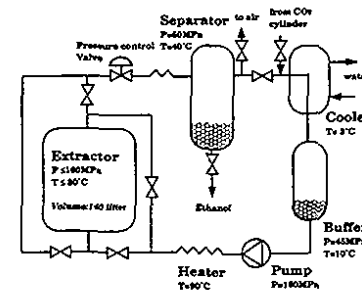

Fig. 5. Flow sheet of the extraction facility at KEK for the production of silica aerogel tiles by super critical CO$_2$.

The standard process pressure and temperature are shown in Fig. 6. The substitution of carbon dioxide for ethanol was performed at a super critical condition of CO$_2$–ethanol system, which is realized, for example, at a pressure of p > 9.35 MP and temperature T = 325.2K [17]. This

substitution takes 14 hours, and the extraction of alcohol proceeds at 15.8 MP and 80°C for 20 hours. Confirming that the ethanol composition in CO_2 is less than 0.3% in the extractor, the pressure of the extractor is gradually decreased to atmospheric pressure in 10 hours. Thus, the whole process takes 47 hours. By employing the super-critical substitution, the probability of having cracks in the aerogels is greatly reduced, and almost 100% of aerogels have no cracks if the thickness is less than 20 mm.
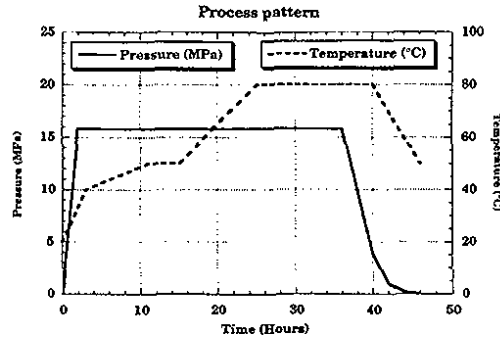

Fig. 6. Process sequence for the pressure and temperature of the CO_2 substitution and drying. The CO_2 substitution is proceeded in a super-critical condition of the CO_2–ethanol system.

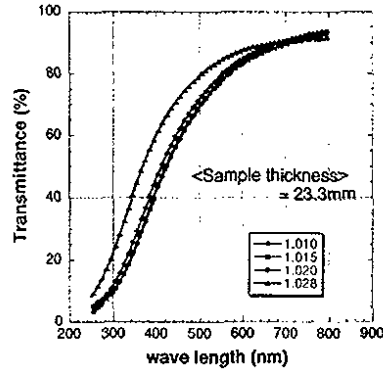

Fig. 7. Light transmittance spectra for the silica aerogels (thickness = 24 mm) of n = 1.01, 1.015, 1.02, and 1.028. The
silica aerogels of n = 1.028, which were prepared by using methanol as the solution, have shown best transmittance.

3.4. Quality

All the aerogel tiles thus produced have been checked for optical transparency, refractive index, density, size, etc. Figure 7 shows a typical transmittance curve obtained by a photo-spectrometer [18] for aerogels of four different refractive indices. The n = 1.028 aerogels have

better transmittance than other ones. Their average transmission length (Λ) at 400nm is 46mm, while others are around 25mm. Here, we define Λ as: $T/T_0 = \exp(-d/\Lambda)$, where T/T_0 is the transmittance, and d is the thickness of the aerogels. These aerogels were produced from the alcogel, which was prepared by using a methanol solution.

The refractive indices are well controlled at $\Delta n/(n-1) \sim 3\%$, which is almost the same as the measurement error. The surface treatment for attaining the hydrophobic property also helps to reduce the shrinkage after drying. Even at n = 1.01 aerogels (density $\rho \sim 0.04$g/cc), the volume shrinkage was only 4%.
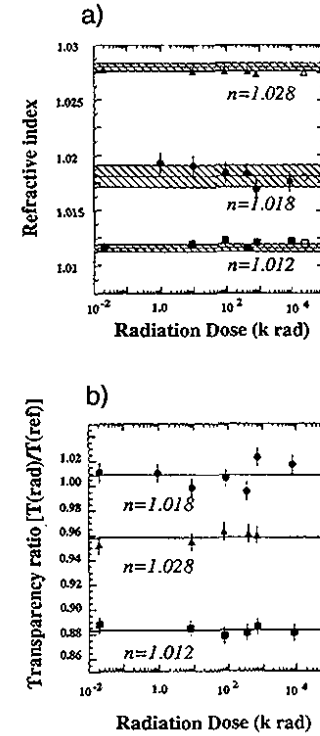

Fig. 8. Effects of radiation dose on aerogels were examined for (a) refractive indices and (b) transparency. In figure 8(a), the solid lines indicate the refractive indices at the production time and the shaded areas are ±1σ regions obtained from the measurements at the production time.

3.5. Radiation Hardness

Detectors will be subject to a high-radiation environment in future high-energy experiments to be carried out at high beam intensity machines. Hence, the radiation hardness of the detectors is a critical issue for such experiments. Radiation damage implies, for instance, that transparent

glasses will turn brown by forming color centers after irradiation. At hadron machines, such as HERA-B, a radiation dose of 10 Mrad/yr. is expected in the vicinity of the beam pipe.

For this reason, we carried out a test to ensure the radiation hardness of aerogels by placing them in high intensity γ-rays from a ^{60}Co source at the irradiation facility in the National Tsing Hua University (Taiwan) [19]. Transparencies and refractive indices of aerogels were measured at several irradiation stages. Up to 9.8 Mrad, which corresponds to more than ten years of running at the KEK B-Factory, no deterioration on the transparency and no change in the refractive indices were observed, as shown in Fig. 8. In order to cancel out effects except the radiation dose, we use transparency ratio, pulse height of the irradiated sample, illuminated by a blue LED normalized by that of nonirradiated sample (reference), which was kept in the same condition (humidity, temperature, etc.) as the irradiated one.
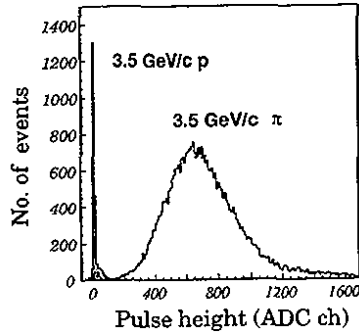

Fig. 9. Pulse height spectra for 3.5 GeV/c pions (above threshold) and protons (below threshold) obtained by a single module of ACC, in which $n = 1.015$ silica aerogels were stacked. Pions and protons are clearly separated by more than 3σ.

4. Performance of the Detector

4.1. Performance of the Single Counter Modules

The performance of single ACC modules has been tested using a 3.5 GeV/c negative pion beam at KEK PS (π 2 beam line). The number of photoelectrons obtained for 3.5 GeV/c pions are 18.2, 20.2, and 20.3 for n = 1.01, 1.015, and 1.02 silica aerogels, respectively. Using equation 3, our photon detection system has higher than 70% efficiency. Typical pulse height distributions for 3.5 GeV/c pions and protons observed by an aerogel counter (n =1.015 with two 2.5" PMT's) are shown in Fig. 9. Pions (above threshold) and protons (below threshold) are clearly separated by more than 3σ. This separation is maintained, even in a high magnetic field (1.5 T). We also found that cracks in the aerogel do not make a difference in the light yield. Although the precursor for the preparation of alcogels is different, our silica aerogels have shown performance as good as the aerogels produced by the Jet Propulsion Lab [20]. In terms of performance in aerogel counters, we believe that there is no significant difference between the aerogel produced by our method and the one produced by the normal two-step method at Caltech.

4.2. Monte Carlo Simulation

In order to arrive at a better understanding of the performance of the aerogel counters, we have developed a Monte Carlo program [21], which can simulate the behavior of Cherenkov photons in the aerogel as realistically as possible. All considerable effects such as Rayleigh scattering, absorption by the aerogel, reflection by the Gortex walls, absorption by the wall, and the response of the PMT's are taken into account as a function of wavelength. The only unknown factor is the absorption in the aerogel, which we have treated as a free parameter and later determined by comparing the results from the simulation with the test beam data. Incident position dependence of the pulse height is compared with the simulation. The absorption length thus determined is about 7 m at λ = 400nm and increases almost exponentially as a function of λ.

5. Other Applications

Since our successful mass-production of silica aerogels, several experimental groups have decided to use silica aerogels for their particle identification devices such as the cosmic antimatter search experiment, the LHC-B experiment, and the internal polarized target experiment (HERMES) [22].

The BESS detector [23], which was launched in a balloon to an altitude of around 10,000m, has successfully completed its role for the observation of antiparticles in primary cosmic rays. Antiprotons are separated from other negatively charged particles by using information from the aerogel Cherenkov counter. A schematic drawing of the BESS detector is shown in Fig. 10. A superconductive solenoid, combined with a tracking system, determines the momenta of charged particles and the signal on the aerogel. Recently, a space station experiment, the Anti-Matter Spectrometer (AMS) has been proposed [24] for a search of antimatter nuclei in space, and it was decided that a silica aerogel Cherenkov counter would be used for isotope separation.
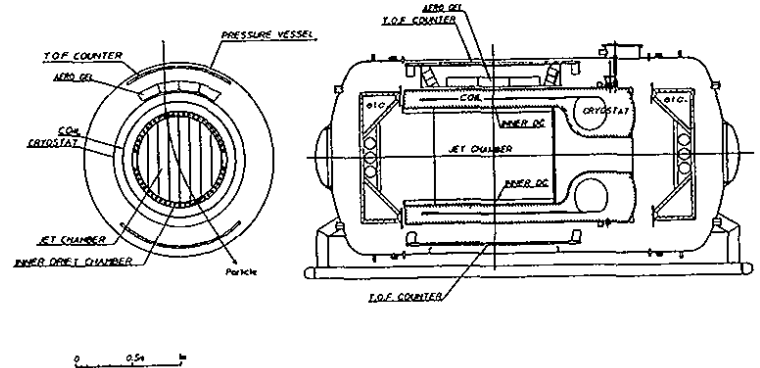

Fig. 10. Layout of the BESS detector. The superconducting solenoidal magnet and the JET-type tracking chamber determines the momenta of charged particles. The TOF and the silica aerogel counters are used for particle identification.

LHC-B and HERMES use aerogels as the radiator for their RICH detectors. Since the scattering length has been improved from the previous one-step aerogels, a clean image of the Cherenkov ring could be observed [25]. We have also succeeded in observing an image of the Cherenkov Ring from our aerogel ($n = 1.03$) radiator of 5 cm thickness, which is shown in Fig. 11. The Cherenkov light was focused on an Image Intensifier (Hamamatsu Photonics Co.) by a concave mirror and recorded on video tapes.
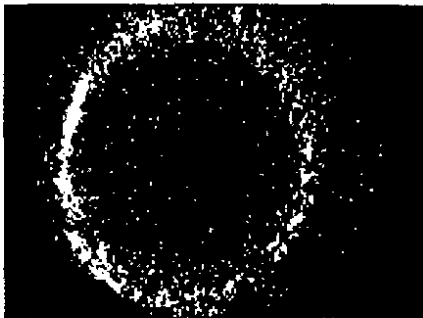

Fig. 11. Ring image of Cherenkov light radiated by 3.5 GeV/c negative pions in the silica aerogel of $n = 1.03$, with a thickness of 5 cm. The image is observed using an image-intensifier. The Cherenkov light was focused by a concave mirror.

6. Conclusion

Silica aerogel is a unique material for threshold-type Cherenkov counter radiators. There are, however, two major difficulties for their application to pion/kaon separation at a momentum range of a few GeV/c. One of the difficulties is achieving a low refractive index ($n < 1.02$) aerogel with high transparency, and the other is long-term stability. The invention of the two-step method and the surface modification to the hydrophobic agent have helped surmount these difficulties. With these advances, good pion/kaon separation is possible up to about 4 GeV/c.

For the BELLE detector at the KEK B-Factory, we have produced about 2 m³ of silica aerogels of $n = 1.01-1.03$ using a new production method. The particle identification capability of the aerogel Cherenkov counters was tested by using real beams. Pion/proton separation of three standard deviations has been achieved. The radiation hardness of aerogels was tested up to 9.8 Mrad. Neither deterioration of transparency or change in the refractive index was observed, which give us confidence in particle identification with aerogels in a high-radiation environment.

Thanks to their improved transparency, namely longer scattering length, aerogels prepared by the two-step method can be used as radiators, for not only threshold-type, but also Ring Imaging Cherenkov counters. Thus, the newly developed aerogel has opened a new era for particle identification in high-energy experiments.

References

[1] C. Arnault et al., Nucl. Instr. and Meth. 177 (1980) 337,

   G. D'Agostini et al., Nucl. Instr. and Meth. 188 (1981) 29,

   S. Henning et al., Phys. Scr. 23 (1981) 703,

   P.J. Carlson et al., Nucl. Instr. and Meth. 192 (1982) 209,

   G. Poelz and R. Riethmüller et al., Nucl. Instr. and Meth. 195 (1982) 491,

   M. Aguilar et al., Nucl. Instr. and Meth. 205 (1983) 79,

   H. Kawai et al., Nucl. Instr. and Meth. 228 (1983) 314,

   P. Vincent et al., Nucl. Instr. and Meth. A272 (1988) 660,

   M. Akei et al., Nucl. Instr. and Meth. A283 (1989) 46,

   C. Lippert et al., Nucl. Instr. and Meth. A333 (1993) 413,

   T. Hasegawa et al., Nucl. Instr. and Meth. A342 (1994) 383.

[2] M. Cartin et al., Nucl. Instr. and Meth. 118 (1974) 177.

[3] A. Linney and B. Peters, Nucl. Instr. and Meth. 100 (1972) 545.

[4] T.M. Tillotson and L.W. Hrubesh, J. Non-Cryst. Solids 145 (1992) 44.

[5] BELLE Collaboration, Letter of Intent for the Belle Collaboration, KEK Report 94-2, 1994.

[6] J.H. Christenson et al., Phys. Rev. Lett. 13 (1964) 138.

[7] M. Kobayashi and T. Maskawa, Prog. Theor. Phys. 49 (1973) 652.

[8] A. Carter and A.I. Sanda, Phys. Lett. 45 (1980) 952.

[9] D. Miller et al., The CLEOIII Detector, CLNS 94/1277.

[10] BABAR Collaboration, BABAR Technical Design Report, SLAC-R-95-457.

[11] T. Lohse et al., HERA B proposal, DESY PRC 94-2.

[12] LHC-B Collaboration, Letter of Intent for LHC-B, CERN/LHCC 95-5 (1995).

[13] Hamamatsu Catalogue, Hamamatsu Photonics K.K., 314-5 Shimokanzo, Toyooka, Shizuoka 438-01, Japan.

[14] Spec. No. 116-027, Japan Goretex Inc., 1-42-5 Akazutsumi, Setagaya, Tokyo 156 Japan.

[15] G. Poelz, Nucl. Instr. and Meth. A248 (1986) 118.

[16] H. Yokoyama and M. Yokogawa, J. Non-Cryst. Solids 186 (1995) 23.

[17] D.W. Jenning, R.J. Lee and A.S. Teja, J. Chem. Eng. Data 36 (1991) 303.

[18] Model U–3210, Hitachi, Ltd., 882 Ichige, Hitachinaka, Ibaraki 312, Japan

[19] S.K. Sahu et al., Nucl. Instr. and Meth. A382 (1996) 441.

[20] We wish to thank James Oyang of Cal Tech for this sample.

[21] R. Suda et al., KEK–Preprint–97–102 (1997).

[22] E. Cisbani at al., "Proposal for a Dual Radiator RICH for Hermes", Hermes Internal Note 97–005 (1997).

[23] K. Anraku et al., KEK–Preprint–94–40 (1994).

[24] S.C.C. Ting et al., Antimatter spectrometer in space, study of feasibility (1994).

[25] R. De Leo et al., CERN–LAA/97-02 (1997). The review article by E. Nappi (SLAC - Journal - ICFA - 17) gives you more information about RICH with aerogel.

A New High-Resolution Time-Of-Flight Technology

P. Fonte, [1,2,*,§] A. Smirnitski, [3] and C. Williams [1,4]

[1] CERN, EP Division, Geneva, Switzerland
[2] LIP-Coimbra, Coimbra, Portugal
[3] ITEP, Moscow, Russia
[4] INFN Bologna, Bologna, Italy

Abstract

In the framework of the ALICE Collaboration, we have recently studied the performance of the multigap Resistive Plate Chambers, which were operated in avalanche mode and at atmospheric pressure for Time-Of-Flight measurements. The detector provided an overall (detector plus electronics) timing accuracy of 120 ps sigma at an efficiency of 98% for MIP's.

The chambers had four 0.3mm gas gaps, limited by both a metallised ceramic plate and a glass plate, with an active dimension of $4 \times 4 cm^2$. The gas mixture contained $C_2H_2F_4 + 5\%isobutane + 10\%SF_6$.

The streamer discharges, each releasing about 20pC at a rate level of a few percent, were tolerated without any noticeable problem.

This detector opens the perspectives for affordable and reliable, high-granularity large area TOF detectors, with efficiency and time resolution comparable to existing scintillator-based TOF technology, but with significantly, a lower price per channel, up to an order of magnitude.

Introduction

The ALICE experiment at the Large Hadron Collider heavy ion program at CERN will include a large area Time-of-Flight (TOF) system, spanning over one hundred square meters with about 100,000 individual read-out channels. Up to 10,000 charged particles are detected per unit of rapidity per event. The TOF technique covers the particle identification of most of these particles. Several types of TOF detectors, including gaseous, have been considered for this application, aiming to provide the required timing accuracy at an affordable cost [1].

One new possibility is the Resistive Plate Chamber (RPC) described in this paper, which was recently developed and tested. Our approach contrasts with a previous application of RPCs to TOF (the Pestov counter [2]) in that we operate a multigap [3] detector in avalanche mode with a nonflammable gas mixture at atmospheric pressure, although at the sacrifice of some timing performance.

* On leave of absence from Instituto Superior de Engenharia de Coimbra, Coimbra, Portugal.
§ Corresponding author; CERN/EP, CH-1211 Geneve 23, Switzerland. (paulo.fonte@cern.ch)

Detector Description

The detector is formed with two identical square-shaped RPC cells, which are electrically connected in parallel. Each cell has an active area of $4\times4cm^2$ and is made of two metallic electrodes placed on each side of a central glass plate, which defines the two gas gaps. No electrical connection is made to the central glass plates, which are made of a commercial variety of dark glass having a resistivity of about $10^{12}\,\Omega\cdot cm$. The metallic electrodes were deposited on profiled ceramic plates [4] and electrical contact was made through a small perforation in the plate, which was placed outside the active gap volume. The width of each gas gap was defined by a set of four spacers placed in the corners of the ceramic plates, located outside the active gap volume. A schematic description of the detector is shown in Figure 1.
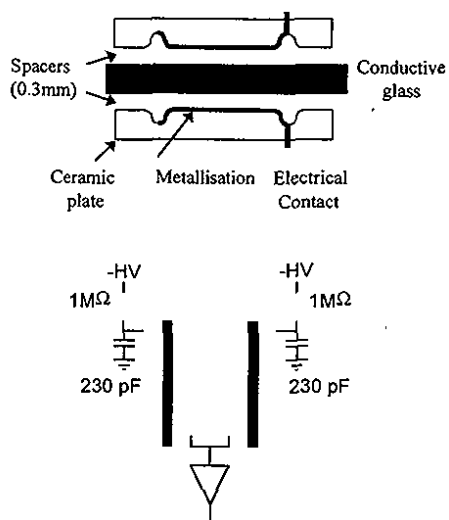

Figure 1 – Schematic representation of the structure of a single RPC cell, made with two metalised, profiled, ceramic plates placed on each side of a central glass plate. Two such cells are electrically connected in parallel to form a single detector.

The chamber signals were amplified by a 2 ns rise-time current amplifier, developed specially for this application [5], followed by a fixed threshold discriminator connected to a TDC with a 50 ps bin width. The output of the amplifier was also sent to a charge integrating ADC that measured the fast signal charge. The charge information was used to correct the finite risetime of the amplifier offline (slewing correction). The noise

contribution of the electronics to the timing jitter was measured to be 50 ps sigma for a signal level of 1.5 pC with a discriminator level of 20 fC.

The detector was filled with a nonflammable gas mixture consisting of $C_2H_2F_4$ + 10% SF_6 + 5% isobutane [6] and tested at the CERN PS using a secondary beam of 7 GeV pions. Two identical scintillation counters provided a time reference with a resolution of 120 ps sigma, and a scintillator-based telescope selected those particles that crossed the detector in a central area of 1 cm^2.
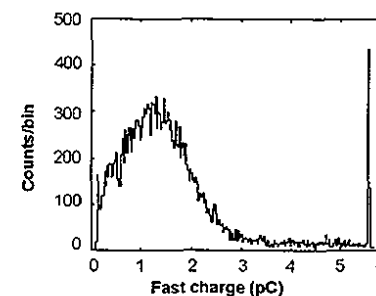

Figure 2 - Fast charge spectrum for MIP's, corresponding to an average charge of 1.5 pC. Above 2 pC the shape of the spectrum is influenced by the nonlinearity of the amplifier.
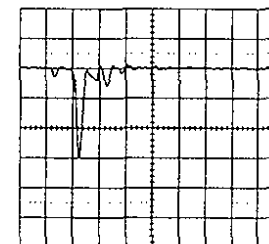

Figure 3 – A typical streamer current pulse, directly observed on a 50 Ω resistor. The horizontal scale corresponds to 20 ns/division and the vertical scale to 1 mA/division. Each square corresponds to a charge of 20 pC. A clear precursory avalanche is visible at 15 ns prior to the main pulse, which corresponds to the development and quenching of the streamer [8].

The fast charge spectrum for minimum ionizing particles is shown in Figure 2, which corresponds to an average fast signal of 1.5 pC in avalanche mode. The sharp left cutoff corresponds to the ADC pedestal, and the narrow peak, which is close to 6 pC, corresponds to the saturation of the ADC. The overall shape of the spectrum, above 2 pC,

is influenced by the nonlinearity of the electronics. About 2% of the particles triggered the formation of streamers, each developing at about 20 pC, and are in qualitative agreement with Ref. 7. A typical streamer pulse is shown in Fig. 3.

In Fig. 4, we show a typical time difference spectrum between the start counters and our detector, with a resolution of 107 ps sigma, after the quadratic subtraction of the start counters contribution (120 ps).
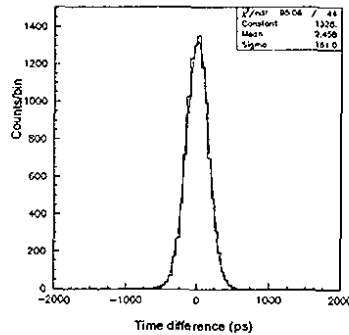

Figure 4 – Typical time difference spectrum between the start counters and our detector, with a resolution of 107 ps sigma, after the quadratic subtraction of the start counters contribution ($\sqrt{161^2 - 120^2} = 107$).

The timing resolution for MIP's was between 100 and 120 ps with a detection efficiency above 98% at counting rates below 800 Hz/cm^2 (see Fig. 5). The performance was degraded at higher counting rates, presumably due to time-dependent voltage drops across the resistive plate.
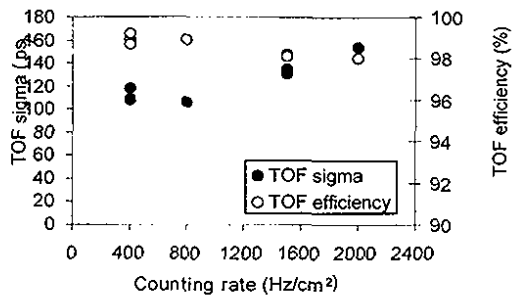

Figure 5 - Timing resolution and efficiency as a function of the counting rate per unit area. For counting rates below 800 Hz/cm^2, resolution of better than 120 ps sigma was achieved with an efficiency above 98%.

Other similar detectors with gas gaps of 0.4 and 0.6 mm were also tested, and the available data (see Fig. 6) suggests that the timing resolution of thin gap parallel geometry detectors depends mainly on the width of the gas gap. One can approximately describe this dependency by a straight line with a slope of 40 ps/0.1 mm.
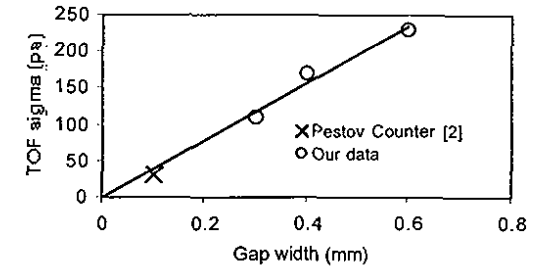

Figure 6 - Tests performed with other detectors featuring different widths of the gas gap suggest that the main contribution to the time jitter is associated to the amplification process in the gas. The timing resolution seems to depend almost linearly on the gap width, with a slope of approximately 40 ps/0.1 mm.

This observation suggests that, in principle, further gains in timing accuracy may be achieved by reducing the gap width. For very small gas gaps, one expects a reduction in efficiency, but this can be compensated by increasing the number of intermediate resistive plates. However, in order to reach timing resolutions comparable to those featured by the Pestov Counter [2] (30 ps sigma), but working in proportional mode and at atmospheric pressure, further progress in electronics must also be made.

Acknowledgment

References

[1] ALICE - Technical Proposal for A Large Ion Collider Experiment at the CERN LHC, CERN/LHCC/95-71, December 1995.

[2] V.V. Parchomchuck, Yu. N. Pestov and N. V. Petrovykh, Nucl. Instrum. Meth. 93 (1971) 269.

[3] E. Cerron Zeballos et al., Nucl. Instrum. Meth. A 374(1996)132.

[4] V. Akimov et al., Nucl. Instrum. Meth. A344 (1994) 120.

[5] R.D'Alessandro et al., Preprint ITEP 51-95 ; A.Martemianov, *Proceedings of the first workshop on electronics for LHC experiments*, Lisbon, 11-15 Sept., 1995.

[6] P. Camarri et al, *Nucl. Instrum. Meth.* A (414)2-3 (1998) 317.

[7] E. Cerron Zeballos et al., *Nucl. Instrum. Meth.* A (411)1 (1998) 55.

[8] H.Raether, *Electron Avalanches and Breakdown in Gases* (London, Butterworths, 1964); P.Fonte et al., *Nucl. Instrum. Meth.* A310, pp.140, 1991; P.Fonte, *IEEE Trans. Nucl. Sci.* vol. 43, pp.2135, 1996.

HIGHLY SEGMENTED LARGE-AREA HYBRID PHOTODIODES WITH BIALKALI PHOTOCATHODES AND ENCLOSED VLSI READOUT ELECTRONICS

A. Braem, E. Chesi, F. Filthaut, A. Go, C. Joram* P. Weilhammer, P. Wicht

CERN, EP Division, Geneva, Switzerland

W. Dulinski

LEPSI, Strasbourg, France

J. Séguinot

Collège de France, Paris, France

H. Wenzel

Phototube consultant, San Ramon, CA, U.S.A.

T. Ypsilantis

INFN Bologna, Italy

ABSTRACT

We report on the principles, design, fabrication, and operation of a highly segmented, large-area hybrid photodiode, which is being developed in the framework of the LHCb RICH project. The device consists of a cylindrical, 127 mm diameter vacuum envelope capped with a spherical borosilicate UV-glass entrance window, with an active-to-total-area fraction of 81%. A fountain-focusing electron optics is used to demagnify the image onto a 50 mm diameter silicon sensor, containing 2048 pads of size 1×1 mm^2. The sensor pads are read out by 16 analogue multiplexed readout chips enclosed in the vacuum envelope. A large ultra-high vacuum plant for the evaporation of visible-light transmittive bialkali (K_2CsSb) photocathodes and subsequent tube encapsulation has been built and successfully operated. The characteristics and performance of the first HPDs have been measured to be in full agreement with expectations.

*Corresponding author. E-mail Christian.Joram@cern.ch.

1   Introduction

Since the BEAUNE 96 conference [1], major progress has been made in the development of Hybrid Photodiodes (HPD). Highly segmented, large-area HPDs have been developed which integrate the readout electronics in the vacuum envelope in order to reduce the number of vacuum feedthroughs needed for the photodetector readout.

At BEAUNE 96, two HPD developments at CERN were presented [2,3], which were still in their first stages. Both developments are carried out in the framework of the Ring Imaging Cherenkov (RICH) detector readout of the LHCb experiment [4].

The development of HPDs constitutes a major advance for the RICH technique because of their

- high granularity, i.e. very large number of pixels (up to ~ 2000), combined with a high spatial resolution;

- sensitivity to visible light, which simplifies the detector construction and results in better performances (merit factor N_0, chromatic aberrations) compared to UV gas detectors;

- excellent energy resolution compared to photomultiplier tubes;

- high rate capability.

These properties make HPDs suitable also for other applications, such as calorimeter readout, fibre tracking or medical imaging [5].

2   The Pad HPD

2.1   The basic design concept

The design of our HPD, which in the following will be called *Pad HPD*, is oriented to the requirements of the readout of the LHCb RICH counters.

An area of about 2.9 m^2 has to be equipped with photodetectors providing high sensitivity (visible and near UV range), single photon detection, a granularity of about 2.5$\times$2.5 mm^2, operation at the LHC bunch crossing rate of 40 MHz, as well as a maximum active area coverage. The resulting high number of readout channels (about 4×10^5) demand the per-channel-cost to be kept below about 10 CHF.

The Pad HPD is a round photodetector of 127 mm (5 inch) diameter (see Fig. 1), with a 114 mm diameter active area visible-light transmissive bialkali photocathode. Hexagonal close packing of the HPDs results in an active area coverage of over 70%. The spherical entrance window of the HPD is made of an UV extended borosilicate glass (T = 50% at $\lambda = 250$ nm). The window and the
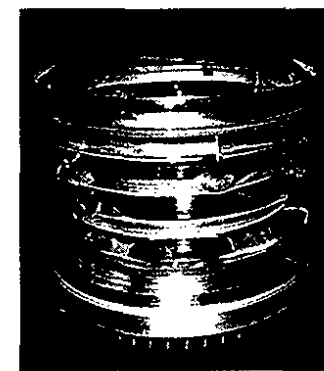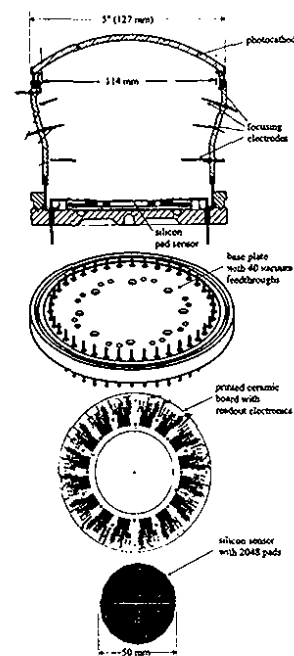

Figure 1: Longitudinal-sectional view and photograph of a sealed Pad HPD with integrated readout electronics.

tube body* are joined by a Kovar skirt in order to adapt to the slightly different thermal expansion coefficients of the glass types. A set of 4 stainless steel ring electrodes defines a fountain shape electrostatic configuration, which demagnifies the photocathode image by a factor ≈ 2.5 onto a silicon sensor of 50 mm diameter. The sensor comprises 2048 pads of size 1×1 mm^2 and is read out by multiplexed analogue electronics enclosed in the vacuum envelope. The resulting readout granularity at the HPD entrance window matches the LHCb requirements. Both the sensor and the electronic chips are mounted on a ceramic carrier, which is wire bonded to the 40 vacuum feedthroughs of the stainless steel base plate.

The design of the Pad HPD is also strongly motivated by the chosen fabrication process (see chapter 3), which consists of an external photocathode evaporation followed by an insitu cold

---

*The vacuum envelope, focusing electrodes and the base plate are fabricated by SVT, F-91170 Viry Chatillon, France.

indium sealing of the base plate to the HPD envelope.

For comparison, the second development project undertaken at CERN aims to produce, in collaboration with industry[†], an 80 mm diameter (sensitive area diameter: 72 mm), cross-focused HPD [6] containing 1024 measurement pixels read out using binary electronics.

2.2 Electron optics

The electrostatic configuration of the Pad HPD is defined in the following way: The electric field between the photocathode (U_C = -20 kV) and the silicon sensor plane (U = 0 V) is shaped by 4 concentric ring electrodes such that the photocathode image is linearly demagnified onto the silicon sensor. The second electrode allows control of the demagnification. The first electrode (the so-called bleeder electrode) corrects nonlinearities and cross-focusing effects at the edge of the cathode. Figure 2 shows electron trajectories in the Pad HPD simulated with the code SIMION[7].
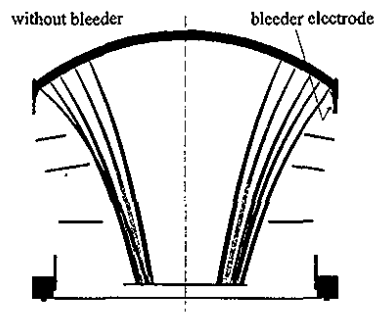
Figure 2: Simulated electron trajectories. Left: Crossing trajectories in a tube without bleeder electrode. Right: Trajectories in a tube with bleeder electrode. For each emission point, photoelectrons with an initial kinetic energy of 1 eV and emission angles of 0° and ±45° are shown.

2.3 The silicon sensor

The sensor consists of a 300μm thick round silicon disk of 52 mm (50 mm active) diameter[‡]. 2048 pads of 980μm ×980μm size are implemented as p$^+$n junctions on the high resistive bulk (5 kΩ·cm).

The spacing between the p$^+$ implants is 40μm. The pads are arranged in 16 sectors in a nearly circular geometry. They are capacitively coupled to readout lines, which are routed on top of a 4μm thick SiO$_2$ insulator to the bonding pads, and are placed at the circumference of the sensor. In the Pad HPD the accelerated photoelectrons impinge on the silicon sensor from the back side. Therefore special care has been taken to minimise the energy loss in the aluminium contact and the nondepleted n$^+$ layer.

2.4 The readout electronics

The Pad HPD is equipped with a low-noise analogue readout chain. An analogue scheme is believed to be crucial for the robust readout of small signals at LHC speed. Compared to a binary readout, lower noise figures can be obtained because disturbances, due to the switching of a comparator, are avoided. The availability of the signal amplitudes provides an efficient and direct way to monitor online the performance of the detector and the readout chain. Instabilities, like gain and noise variations or common mode noise effects, can be handled by continuously updating the pedestal average and variance using Digital Signal Processors (DSP). The analogue readout exploits the excellent energy resolution which is one of the most attractive features of the HPD principle and which can be used to recognize multiple photoelectrons in the pattern recognition in high density RICH images.

To realise a HPD with a high number of readout channels, the readout electronics is enclosed in the vacuum envelope. The number of vacuum feedthroughs is kept at a technically feasible number by signal multiplexing. Apart from a low power consumption, compatibility with typical ultra-high vacuum bake-out cycles and negligible long term outgassing are indispensable. The fact that the electronics can be positioned very close to the Si sensor represents a major advantage in view of the very small signal of less than 1fC created by single photoelectrons in the sensor. Minimal capacity at the amplifier input is essential for the lowest possible noise and a stable operation.

The measurements presented in this paper have been obtained with the Viking VA3 electronics [8]. The VLSI chip comprises, for each of its 128 channels, a front-end charge amplifier, a shaper, and a sample-and-hold unit, which determines the maximum amplitude of the shaped signal. The power consumption is $\approx$ 300μW/channel. The VA3 with a shaping time of 1.3μs is clearly too slow to be used at LHC. Therefore, a low capacity (LC) version of the analogue SCTA128 chip [9] has been developed, which will be used in the final Pad HPD. The chip provides signal shaping with a peaking time of 25 ns and also incorporates the LHC-specific features like a 128 cell deep analogue pipeline, a derandomising buffer (8 cells deep) and 40 MHz analogue multiplexing. Tests with the recently available SCTA128LC chip demonstrated the design peaking time and the fast multiplexing. From measurements where the SCTA128LC was connected to a small silicon sensor,

pedestal noise values as low as 600 to 700 e^- are expected when connected to a Pad HPD sensor. The integration of the SCTA128LC in the Pad HPD is foreseen in the next months.

3 Fabrication of the Pad HPD

The Pad HPD fabrication uses an external photocathode evaporation process (sometimes referred to as transfer technique) followed by an insitu encapsulation of the tube with the base plate, using a cold indium sealing technique. The silicon sensor and the readout electronics are mounted on the base plate prior to the evaporation process. During the cathode processing, the base plate is kept at a safe distance from the envelope. This technique was chosen:

- to avoid a destructive contamination of the silicon sensor and the readout electronics by the alkali metal vapours (K, Cs) during the evaporation process;
- to minimise the thermal load on the sensor and electronics during the bakeout procedure and the sealing, which could lead to irreversible damage to the semiconductor material.

A further advantage of the technique is the possibility to reopen sealed tubes, which do not operate with a satisfactory performance. It has been demonstrated that all HPD components, in particular the relatively expensive silicon sensor and electronics chips, can be reused after such an intervention.

3.1 Photocathode processing

In the literature various processes are described to produce semi-transparent bialkali (K_2CsSb) photocathodes. The processes can be divided into two classes: Sequential processes, where antimony and then the alkali metals are evaporated one after the other, and co-evaporation processes, where usually Sb and K are evaporated simultaneously. Numerous variants exist, which differ mainly in the number and order of the steps and the substrate temperature cycle. The details of a process depend on many parameters (e.g., geometrical configuration of the substrate and the evaporation sources, temperature gradients, pumping conductance) and have always to be determined by iterative optimisation. We have adopted a co-evaporation process which comprises about 20 individual evaporation steps. In comparison to the simpler sequential processes, co-evaporation permits a reduction in the amount of evaporated materials. This reduces the contamination of the tube with alkali films which may lead to a degradation of the high voltage capability of the sealed tube.

The Pad HPD is fabricated in a large ultra-high vacuum plant which has been designed and built at CERN [10]. After a bake-out at 160°C, the plant reaches ultimate pressures of a few 10^{-10} mbar. The pressure at the start of the photocathode processing, when the vacuum tank is kept at an elevated temperature, is typically 2×10^{-9} mbar. The composition of the residual gas is monitored by means of a quadrupole mass spectrometer. Care is taken to keep the partial pressures of water and any other reactive substances (O_2, CO) below 1×10^{-9} mbar. The residual gas consists to about 90% of hydrogen which is outgassing from the stainless steel walls. An internal tubular heating spiral is used to bake out the HPD envelope at a temperature of about 300°C, which is necessary to fully remove water also from the bulk of the tube envelope. The evaporation plant is controlled by a distributed slow control system under PC control[§].

The envelope is mounted on a rigid support structure in the centre of the tank. A transfer system allows a carriage which is equipped with the three evaporation sources to be positioned such that the sources sit close to the centre of curvature of the spherical tube window. During the processing, the envelope is kept at a constant temperature of 150°C.

The evolution of the photocathode sensitivity is monitored online by measuring the photocurrent between the photocathode and the focusing ring electrodes (anode), where a collection voltage of typically 100 V is applied. The cathode is exposed to white or monochromatic light of precisely known intensity. Knowledge of the true photocurrent, i.e., the quantum efficiency, and possible background currents, is essential for the optimisation of the photocathode.

3.2 Tube encapsulation

A cold indium sealing technique has been developed to encapsulate the envelope with the base plate. The method requires a number of preparatory steps. An indium wire of 99.99% purity is placed in the circular V-shaped groove on the base plate. A 10 μm thick nickel layer was galvanically deposited on the groove surface to improve the wetting and uniformity of the indium. Heating the baseplate in a dedicated set-up under vacuum at 250°C melts the indium. The liquid indium is stirred under vacuum by means of a rotating needle in order to completely degas it and further improve its uniformity. The contact surface of the envelope, i.e., the knife edge of the envelope's flange, is deposited with a 10 μm thick nickel layer and an evaporated gold film of 500 nm thickness.

Once the pretreatment is finished, and the silicon sensor and the electronics are mounted and wire bonded to the vacuum feedthroughs on the base plate, the base plate is installed in the photocathode evaporation plant on a second movable carriage. The tube encapsulation is performed several hours after the photocathode processing, when the cathode has cooled down to room temperature. The carriage is then aligned under the envelope. A press mechanism allows the base plate to be pushed gradually against the flange of the envelope with a force of 25 kN. The knife edge cuts into the indium filled groove. The high mechanical pressure associated with this technique results in perfectly tight vacuum seals, which do not require additional clamping.

[§]Fieldpoint I/O system, BridgeView software, National Instruments

4 Performance

Numerous measurements characterising the HPD have been performed. We present quantum efficiency measurements, which have been obtained online during the photocathode evaporation, and subsequently a number of measurements, where the sealed HPD has been exposed to a low intensity H_2 flash lamp. The narrow spot of the flash lamp ($\sigma \approx 1$ mm) can be precisely scanned over the HPD window by means of a movable mirror.

4.1 Quantum efficiency of the K_2CsSb photocathodes

The quantum efficiency is measured online during the photocathode evaporation. Light from a tungsten halogen lamp is focused through a viewport in the vacuum tank onto the HPD entrance window. A set of interference filters (combined with appropriate broad band pass filters) provides a selection of wavelengths between 308 nm (4 eV) and 651 nm (1.9 eV). The intensity of each individual wavelength is determined by means of a calibrated photodiode. The light is chopped by an electronic shutter so that any background can be subtracted. The quantum efficiency is then measured in DC current mode by applying a voltage of typically 100 V between the photocathode and the focusing ring electrodes. Figure 3, left, shows the quantum efficiency of a recently produced HPD. It reaches a maximum of about 20% around 350 nm. All recently produced cathodes had peak quantum efficiencies between 15% and 20%. The further optimisation of the quantum efficiency is the subject of current studies. The light spot, which has a size of about 2 cm² can be scanned over the window surface. The uniformity of the efficiency is typically better than ±10%, where part of it may be due to a nonuniform and incomplete collection efficiency with the field configuration used. A clarification of this point will follow from measurements with a Cherenkov radiator. Devices which had been subject to correct baking of the vacuum plant and the HPD components, have shown no measurable degradation of the quantum efficiency over time scales of months.

4.2 Electron optical parameters

Although the design value for the tube high voltage is 20 kV, the detector has been stably operated at up to 30 kV. The fountain shape field configuration is able to produce an almost purely linear imaging over the full active diameter (114 mm). The demagnification factor can be adjusted by varying the voltage of the second electrode. Figure 3, right, shows the correlation between the radial coordinate of the light spot on the photocathode and the centre of gravity of the charge distribution on the silicon sensor. The slope of a linear curve fitted to the data gives a demagnification of 2.7. The fit residuals of typically 200 μm can be reduced to about 50 μm by allowing a superposition of two linear curves.
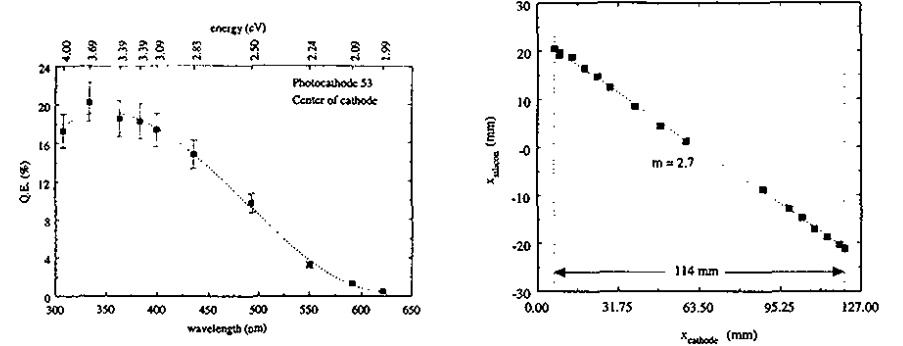

Figure 3: Left: Quantum efficiency versus wavelength of a recently produced HPD. Right: Correlation between the photon detection point and the centre of gravity of the charge distribution measured on the silicon sensor.

The point spread function, i.e., the spatial distribution of the photoelectrons on the silicon anode originating from a point-like spot on the photocathode, is difficult to determine with our current set-up, because of the comparably large light spot and (for this purpose) the relatively coarse granularity of the silicon sensor. From fitting the charge distribution of single photoelectrons on the silicon sensor and unfolding the contributions of the spot size and the granularity of the sensor, for 20 kV a point spread function with a Gaussian width of 400 μm is found. This is to compared with the pixelization error $\sigma_{pixel} = 1$ mm $/\sqrt{12} = 288$ μm. For voltages above 23 kV, the point spread contribution is less than the pixel error.

4.3 Signal characteristics

An HPD provides perfect linearity between the signal amplitude and the voltage applied between the anode and cathode. Figure 4, left, shows the signal amplitude for single photoelectrons in ADC channels, as a function of the anode-cathode voltage. The intersection with the horizontal axis at 0.53 kV corresponds to an energy loss of only 530 eV in the backplane metallisation and the non-depleted n^+ layer of the silicon. The ADC calibration follows from the slope of the curve (3.929 ADC bins/kV) and the energy required to create an electron-hole pair (in the following, simply called electrons or e^-) in silicon (3.62 eV/e^-): 1 ADC bin = 70.3 e^-. A pulse height spectrum at 20 kV is shown in Fig. 4, right. The pedestal, which has a Gaussian width of $\sigma_{noise} = 4.04$ ADC bins or 285 e^-, has been subtracted and a $4\sigma_{noise}$ cut has been applied. The single photoelectron peak appears at 77.5 ADC counts (5.02 ADC counts width). The signal-to-noise ratio is 19. The

background in Figure 4, right, is due to the characteristic backscattering of photoelectrons from the silicon surface, which occurs with a probability of about 18%. Assuming a uniform distribution of the deposited energy of back-scattered photoelectrons between 0 and the full energy, the single *photoelectron detection efficiency is expected to be 94%.*
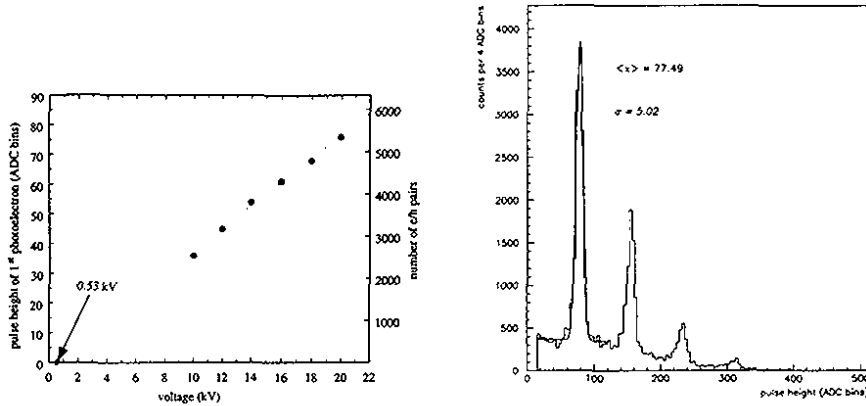

Figure 4: Left: Measured signal amplitude for single photo-electrons versus anode-cathode voltage. Right: Measured pulse height spectrum in ADC counts at 20 kV for an average number of photoelectrons of 0.9. The pedestal has been subtracted and a $4\sigma_{noise}$ cut has been applied.

5 Status and outlook

The first sealed HPDs with bialkali photocathodes and integrated readout electronics have been fabricated and successfully tested. The performance of the detectors is in good agreement with the design expectations and makes it an excellent candidate for the LHCb RICH detector readout. Whereas the past year has been mainly devoted to developing the complex production technologies, we are now in the phase of fine tuning the various parameters, in order to further optimise the quantum efficiency of the photocathode and the production yield. In parallel, preparatory work is going on in order to fabricate HPDs with the fast SCTA128 electronics still in 1999. A test of the HPD in a Cherenkov radiator set-up, which is scheduled for July 1999, will be used to further characterise the performance of the detector.

References

[1] R. DeSalvo, Nucl. Instr. Meth. A387 (1997) 92.

[2] E. Chesi et al., Nucl. Instr. Meth. A387 (1997) 122.

[3] T. Gys et al., Nucl. Instr. Meth. A387 (1997) 131.

[4] LHCb Technical Proposal, CERN/LHCC 98-4, LHCC/P4, 1998.

[5] C. Joram, Proceeding of the VIth Int. Conf. on Advanced Technology and Particle Physics, Como, Italy, 1998, in press.

[6] M. Alemi et al., Proceeding of the 1998 Nuclear Science Symposium and Medical Imaging Conference, Toronto, Canada, 1998, in press.

[7] D. Ferenc, Proceeding of the 1998 Nuclear Science Symposium and Medical Imaging Conference, Toronto, Canada, 1998, in press.

[8] P. Weilhammer et al., Nucl. Instr. Meth. A384 (1996) 159.

[9] F. Anghinolfi et al., IEEE Transactions Nucl. Sci., Vol. 44, No 3 (1997) 298.

[10] E. Chesi et al., LHCb note, 98-007 RICH.